An equilibrium-based formulation with nonlinear configuration dependent interpolation for geometrically exact 3D beams

Murillo Santana, Carlo Sansour, Mohammed Hjiaj, Hugues Somja

An equilibrium-based formulation with non-linear configuration dependent interpolation for geometrically-exact 3D beams

M. V. B. Santana*[1] | C. Sansour[1,2] | M. Hjiaj[1] | H. Somja[1]

[1]LGCGM/Structural Engineering Research Group, INSA de Rennes, Rennes, France
[2]Department of Computational Sciences & Engineering, Bethlehem University, Bethlehem, Palestine

Correspondence
*M. V. B. Santana. Email: mbentosa@insa-rennes.fr

Abstract

This paper describes a novel equilibrium-based geometrically-exact beam finite element formulation. First, the spatial position and rotation fields are interpolated by non-linear configuration-dependent functions that enforce constant strains along the element axis, completely eliminating locking phenomena. Then, the resulting kinematic fields are used to interpolate the spatial sections force and moment fields in order to fulfill equilibrium exactly in the deformed configuration. The internal variables are explicitly solved at the element level and closed-form expressions for the internal force vector and tangent stiffness matrix are obtained, allowing for explicit computation, without numerical integration. The objectivity and absence of locking are verified and some important numerical and theoretical aspects leading to a computationally efficient strategy are highlighted and discussed. The proposed formulation is successfully tested in several numerical application examples.

KEYWORDS:
Geometrically-exact beam, Equilibrium-based formulation, Locking-free beam element, Finite element formulation

1 | INTRODUCTION

A large variety of engineering systems can be modeled accurately as an assembly of beam elements. Currently, spatial beam finite element formulations can be divided in three categories: Co-rotational (CR), Total Lagrangian (TL) and Updated Lagrangian (UL), the former two being most active topics of research in the last decades. Co-rotational formulations focus on filtering the rigid-body motion from the element total displacements and rotations, computing the internal forces and tangent stiffness from the remaining deformation part of the motion and applying a transformation that bring back this quantities to the global system [12]. On the other hand, Total Lagrangian formulations focus on describing the exact kinematics of the element, along with the relevant strain measures and then directly computing the global internal forces and tangent stiffness [38].

The geometrically-exact beam theory, introduced by Simo [38], considers that the beam sections move as a rigid-body and can then be described by position and rotation fields. This theory has been studied by many researchers, e.g. [2, 7, 11, 47], forming a base for TL spatial beam finite element formulations. In TL formulations, the exact kinematics of the element is described and so, all the non-linear coupling effects are directly captured by the element [46]. However, traditional interpolation schemes for the position and rotation fields used in linear analysis leads to shear, bending and membrane locking phenomena [39]. Moreover, as shown by Jelenić and Crisfield [15], although the strain measures derived in the geometrically-exact beam theory are invariant under rigid-body motion, the same quantities in a finite element with traditional interpolation are not, causing the formulation to lose objectivity.

This article has been accepted for publication and undergone full peer review but has not been through the copyediting, typesetting, pagination and proofreading process which may lead to differences between this version and the Version of Record. Please cite this article as doi: 10.1002/nme.6862

Methodologies for reducing or eliminating locking phenomena in beams TL formulations have been investigated by many researchers in the recent years. In the original contribution, Simo and Vu-Quoc [39] used reduced integration as an alternative to mitigate locking. Weeger et al. [44, 45] and Magisano et al. [18] adopted isogeometric analysis for the higher-order interpolation of the position and rotation fields. In this methodology it's possible to elevate the order of the shape functions, reducing the locking effects but not completely removing it. Romero [28] investigated the influence of the rotation interpolation on the response of geometrically-exact beam elements. Cardona and Geradin [6] defined an interpolation method based on the increments of the rotations.

Meier et al. [20, 21, 22] adopted a curved Kirchhoff rod model to develop a shear free beam formulation. Ghosh and Roy [13] studied a consistent quaternion interpolation for objective finite element approximation. Sansour and Wagner [30] proposed a multiplicative updating of the rotation tensor in the finite element analysis of rods and shells. Zupan and Saje [48] investigated the integration of rotation from angular velocity, while Treven and Saje [43] studied the integration of rotation and angular velocity from curvature. Park and Ravani [24] derived a smooth invariant interpolation for rotation tensors. Crisfield and Jelenić [10] and Jelenić and Crisfield [15] proposed an interpolation of the rotation field constructed on the SO(3) space and based on the relative rotation of the beam nodes, yielding a constant curvature strain. Sonneville et al. [40, 41] proposed an interpolation of the position and rotation fields constructed in the SE(3) space via the exponential map of the related Lie algebra, yielding constant shear and constant curvature strains. Rong et al. [29] used a SE(3) formulation for thin-walled beams considering warping. Mäkinen [19] developed a Reissner's geometrically exact beam element without singularities. Sansour et al. [31] studied an energy-moment method for Euler-Bernoulli beam dynamics. Boyer and Primault [5] investigated slender beams via finite transformations.

In terms of hybrid-mixed finite element formulations, the non-linear coupling between the sections kinematic and stress-resultant fields, associated with the geometrically-exact beam theory, creates a difficulty in obtaining equilibrium-based interpolations. In the literature, most attention have been dedicated to geometrically linear formulations immersed in CR frameworks. Ayoub and Filippou [3] developed a non-linear mixed formulation for the analysis of steel-concrete composite beams. Saritas and Filippou [36] studied inelastic axial-bending–shear coupling with mixed formulations. Alsafadie et al. [1] improved existing an CR formulation to take into account shear and warping deformations in thin-walled beams. Santos and de Almeida [34] developed a equilibrium-based TL finite element formulation for geometrically-exact planar beams. Santos et al. [33] studied hybrid and multi-field variational principles for geometrically exact three-dimensional beams. Santos et al. [35] developed a TL geometrically-exact beam formulation with low order interpolation of the kinematic fields and equilibrium-based interpolation of the resultant fields. Ritto-Corrêa and Camotim [27] determined the work-conjugacy between rotation-dependent moments and finite rotations.

A novel approach is presented in this work, where an equilibrium-based geometrically-exact TL beam formulation is developed. Locking phenomena in a finite element formulation is directly related to the inability to independently represent low-order deformation modes. In the present formulation, locking phenomena is completely eliminated by adopting non-linear configuration-dependent interpolation functions that enforce constant shear and curvature strains along the element axis. The obtained interpolated strain measures are also shown to be invariant under rigid-body motion. Moreover, in order to further increase the accuracy of the formulation, an equilibrium-based method is adopted, enriching the spatial force and moment fields. Closed-form expressions for the internal force vector and tangent stiffness matrix are obtained, without requiring numerical integration and so yielding a computationally efficient finite element formulation. The development of such a beam formulation is unprecedented and original to the authors best knowledge.

The main objective of the present contribution is to combine the best features of the CR and TL approaches by developing a locking-free equilibrium-based geometrically-exact beam element with configuration-dependent interpolation functions, therefore preserving the high-performance properties of standard linear analysis formulations while considering the geometrically-exact kinematics of the motion. For this, the non-linear configuration-dependent interpolation functions are obtained by enforcing constant strains along the element axis. The spatial force and moment fields are interpolated exactly fulfilling the equilibrium equations at each section in the deformed configuration. Finally, closed-form expressions for the internal force vector and tangent stiffness matrix are derived.

The main originalities of the present contribution are:

- Non-linear configuration-dependent interpolation of the spatial forces and moments, exactly fulfilling the equilibrium equations at the current (deformed) configuration;

- Explicit elimination of the internal variables (stress-resultants) at the element level, avoiding singularity issues usually associated with mixed-hybrid methods;

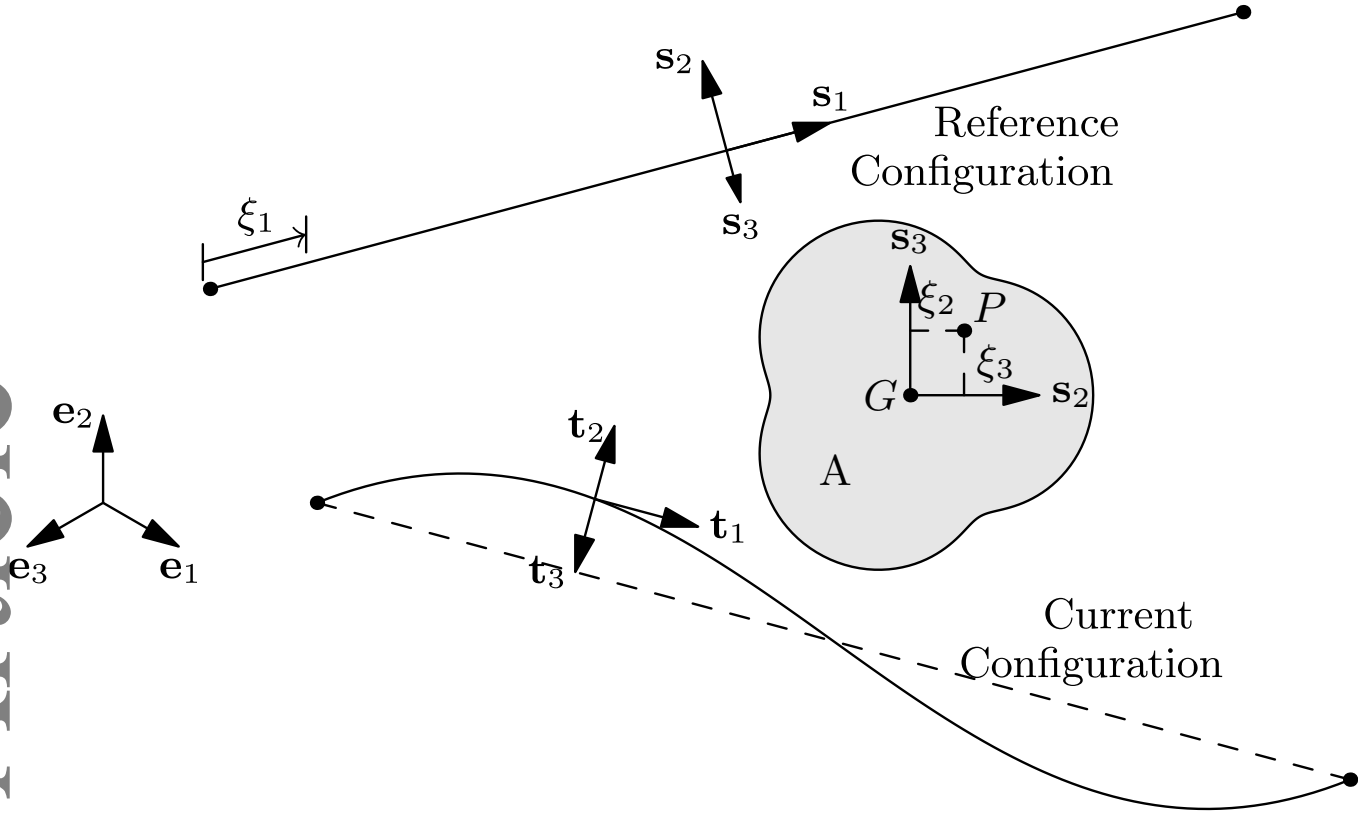

FIGURE 1 Beam element in the reference and current configurations.

- Efficient closed-form expressions for the internal force vector and tangent stiffness matrix, avoiding the use o numerical integration and so considerably reducing the computational time.

The paper is structured as follows. In Section 2 the fundamentals aspects of the geometrically-exact beam theory are reviewed. In Section 3, the interpolation functions for the position and rotation fields are derived by enforcing constant strains in the element in order to avoid locking phenomena. In Section 4, the spatial force and moment fields are interpolated by enforcing strong equilibrium. The internal variables are explicitly determined at the element level and expressions for the internal force vector and tangent stiffness matrix are derived. Section 5 presents a number of numerical applications, highlighting the accuracy and efficacy of the proposed formulation. Finally, in Section 6, some conclusions and suggestions for future works are given. For completeness, some basic relations of spatial rotations are included in A.

2 | GEOMETRICALLY-EXACT BEAM THEORY

The geometrically-exact beam theory introduced by Simo [38] is considered in the present work. The beam is treated as a prismatic body, described with arc-length parameter $\xi_1 \in [0, L]$ and section mapping $(\xi_2, \xi_3) \in A$ (Fig. 1). For the sake of simplicity, it's assumed that the beam is straight in the reference configuration, with axial direction $\mathbf{s}_1$ and section principal axes $\mathbf{s}_2$ and $\mathbf{s}_3$. The beam's sections move as a rigid body, with the position of the center of gravity G specified by the curve $\mathbf{x}(\xi_1) \in \mathbb{R}^3$ and orientation described by the rotation tensor $\mathbf{R}(\xi_1) \in \mathrm{SO}(3)$. The position $\mathbf{x}_p(\xi_1, \xi_2, \xi_3)$ of a general material point P can then be written as:

$$\mathbf{x}_p(\xi_1, \xi_2, \xi_3) = \mathbf{x}(\xi_1) + \mathbf{R}(\xi_1)\left(\xi_2\mathbf{s}_2 + \xi_3\mathbf{s}_3\right) \tag{1}$$

Taking the derivative of the current configuration with respect to the initial one, the deformation gradient $\mathbf{F}$ can be obtained as:

$$\mathbf{F} = \mathbf{R}\left(\mathbf{I} + \boldsymbol{\Upsilon} \otimes \mathbf{s}_1\right) \tag{2}$$

where:

$$\widehat{\mathbf{\Omega}} = \mathbf{R}^T\mathbf{R}' \tag{3}$$

$$\mathbf{\Gamma} = \mathbf{R}^T\mathbf{x}' - \mathbf{s}_1 \tag{4}$$

$$\mathbf{\Upsilon} = \mathbf{\Gamma} + \xi_2\mathbf{\Omega}\times\mathbf{s}_2 + \xi_3\mathbf{\Omega}\times\mathbf{s}_3 \tag{5}$$

Throughout the paper, $(\bullet)'$ denotes the derivative with respect to the arc-length parameter ξ_1 and $\widehat{(\bullet)}$ represents the skew-matrix obtained from $\mathbb{R}^3$ vectors. The sections translational deformation $\mathbf{\Gamma}$ (Eq. 3) is composed by stretch ($\Gamma_1 = \mathbf{\Gamma}\cdot\mathbf{s}_1$) and shear ($\Gamma_2 = \mathbf{\Gamma}\cdot\mathbf{s}_2$, $\Gamma_3 = \mathbf{\Gamma}\cdot\mathbf{s}_3$) deformations. The sections rotational deformation (curvature) $\mathbf{\Omega}$ (Eq. 4) comprises torsion ($\Omega_1 = \mathbf{\Omega}\cdot\mathbf{s}_1$) and bending ($\Omega_2 = \mathbf{\Omega}\cdot\mathbf{s}_2$, $\Omega_3 = \mathbf{\Omega}\cdot\mathbf{s}_3$) deformations [38]. The sections deformations $\mathbf{\Gamma}$ and $\mathbf{\Omega}$ (and consequently the deformation vector $\mathbf{\Upsilon}$) are invariant under superimposed rigid body motion. In fact, if a constant rotation $\mathbf{Q}$ and constant displacement $\mathbf{c}$ are imposed over the current configuration, the new configuration ($\mathbf{x}^*$, $\mathbf{R}^*$) can be expressed as:

$$\mathbf{R}^* = \mathbf{Q}\mathbf{R} \tag{6}$$

$$\mathbf{x}^* = \mathbf{Q}\mathbf{x} + \mathbf{c} \tag{7}$$

and the corresponding section's deformations are:

$$\widehat{\mathbf{\Omega}}^* = \mathbf{R}^T\mathbf{Q}^T\mathbf{Q}\mathbf{R}' = \mathbf{R}^T\mathbf{R}' = \widehat{\mathbf{\Omega}} \tag{8}$$

$$\mathbf{\Gamma}^* = \mathbf{R}^T\mathbf{Q}^T\mathbf{Q}\mathbf{x}' - \mathbf{s}_1 = \mathbf{R}^T\mathbf{x}' - \mathbf{s}_1 = \mathbf{\Gamma} \tag{9}$$

The Green-Lagrange strain tensor can then be obtained as:

$$\mathbf{E} = \frac{1}{2}\left(\mathbf{F}^T\mathbf{F} - \mathbf{I}\right) \tag{10}$$

$$\mathbf{E} = \left(\mathbf{\Upsilon}\cdot\mathbf{s}_1 + \frac{\mathbf{\Upsilon}\cdot\mathbf{\Upsilon}}{2}\right)\mathbf{s}_1\otimes\mathbf{s}_1 + \sum_{k=2}^{3}\frac{\mathbf{\Upsilon}\cdot\mathbf{s}_k}{2}\left(\mathbf{s}_1\otimes\mathbf{s}_k + \mathbf{s}_k\otimes\mathbf{s}_1\right) \tag{11}$$

From the kinematic assumption of section's rigid-body motion, the following out-of-plane components of deformation are identically null:

$$E_{22} = \mathbf{s}_2\cdot\mathbf{E}\mathbf{s}_2 = 0 \tag{12}$$

$$E_{33} = \mathbf{s}_3\cdot\mathbf{E}\mathbf{s}_3 = 0 \tag{13}$$

$$E_{23} = \mathbf{s}_2\cdot\mathbf{E}\mathbf{s}_3 = 0 \tag{14}$$

The section's shear deformations, E_{12} and E_{13}, can be obtained as:

$$E_{12} = \mathbf{s}_1\cdot\mathbf{E}\mathbf{s}_2 = \frac{\mathbf{\Upsilon}\cdot\mathbf{s}_2}{2} = \frac{1}{2}\left(\Gamma_2 - \xi_3\Omega_1\right) \tag{15}$$

$$E_{13} = \mathbf{s}_1\cdot\mathbf{E}\mathbf{s}_3 = \frac{\mathbf{\Upsilon}\cdot\mathbf{s}_3}{2} = \frac{1}{2}\left(\Gamma_3 + \xi_2\Omega_1\right) \tag{16}$$

The axial strain E_{11} can be written as:

$$E_{11} = \mathbf{s}_1\cdot\mathbf{E}\mathbf{s}_1 = \mathbf{\Upsilon}\cdot\mathbf{s}_1 + \frac{\mathbf{\Upsilon}\cdot\mathbf{\Upsilon}}{2} \tag{17}$$

As the section's deformations $\mathbf{\Gamma}$ and $\mathbf{\Omega}$ (and consequently the deformation vector $\mathbf{\Upsilon}$) represents true deformation measures, the higher-order term $\mathbf{\Upsilon}\cdot\mathbf{\Upsilon}/2$ can be neglected by assuming small strains while preserving the notion of large displacements and rotations in the beam element. The axial strain E_{11} is then given by:

$$E_{11} = \Gamma_1 - \xi_2\Omega_3 + \xi_3\Omega_2 \tag{18}$$

The equilibrium of the element can be stated via the virtual work relation $\delta U = \delta V$ [38], where δU and δV represent the internal and external virtual work, respectively. Considering distributed forces $\overline{\mathbf{n}}(\xi_1)$ and moments $\overline{\mathbf{m}}(\xi_1)$ acting along the beam span, as well as concentrated forces ($\mathbf{n}_1$ and $\mathbf{n}_2$) and concentrated moments ($\mathbf{m}_1$ and $\mathbf{m}_2$) acting on the end nodes, the external virtual work can be written as:

$$\delta V = \int_0^L \left(\overline{\mathbf{n}}\cdot\delta\mathbf{x} + \overline{\mathbf{m}}\cdot\delta\boldsymbol{\theta}\right)d\xi_1 + \mathbf{n}_1\cdot\delta\mathbf{x}_1 + \mathbf{m}_1\cdot\delta\boldsymbol{\theta}_1 + \mathbf{n}_2\cdot\delta\mathbf{x}_2 + \mathbf{m}_2\cdot\delta\boldsymbol{\theta}_2 \tag{19}$$

The internal virtual work δU can be obtained by taking the inner product of the second Piola–Kirchhoff stress tensor $\mathbf{S}$ with the variation of the Green-Lagrange strain tensor $\delta\mathbf{E}$ as:

$$\delta U = \int_0^L \int_A \left(S_{11}\delta E_{11} + 2S_{12}\delta E_{12} + 2S_{13}\delta E_{13} \right) dA d\xi_1 \tag{20}$$

Integrating over the section domain, we obtain:

$$\delta U = \int_0^L \left(\mathbf{N}\cdot\delta\boldsymbol{\Gamma} + \mathbf{M}\cdot\delta\boldsymbol{\Omega} \right) d\xi_1 \tag{21}$$

where the section resultants are defined as:

$$N_1 = \mathbf{N}\cdot\mathbf{s}_1 = \int_A S_{11} dA \tag{22}$$

$$N_2 = \mathbf{N}\cdot\mathbf{s}_2 = \int_A S_{12} dA \tag{23}$$

$$N_3 = \mathbf{N}\cdot\mathbf{s}_3 = \int_A S_{13} dA \tag{24}$$

$$M_2 = \mathbf{M}\cdot\mathbf{s}_2 = \int_A +\xi_3 S_{11} dA \tag{25}$$

$$M_3 = \mathbf{M}\cdot\mathbf{s}_3 = \int_A -\xi_2 S_{11} dA \tag{26}$$

$$M_1 = \mathbf{M}\cdot\mathbf{s}_1 = \int_A \left(\xi_2 S_{13} - \xi_3 S_{12} \right) dA \tag{27}$$

If an elastic response (with Young E and shear G modulus) is considered, under the hyper-elastic Saint Venant–Kirchhoff material model, we have:

$$S_{11} = E E_{11} \tag{28}$$

$$S_{12} = G E_{12} \tag{29}$$

$$S_{13} = G E_{13} \tag{30}$$

Combining Eqs. (22) - (27) with Eqs. (28) - (30) and integrating over the section domain A, the resultants $\mathbf{N}$ and $\mathbf{M}$ can be directly obtained from the deformations $\boldsymbol{\Gamma}$ and $\boldsymbol{\Omega}$ as:

$$\mathbf{N} = \mathbf{C}\boldsymbol{\Gamma} \tag{31}$$

$$\mathbf{M} = \mathbf{D}\boldsymbol{\Omega} \tag{32}$$

where the elastic tensors $\mathbf{C}$ and $\mathbf{D}$ are related to the section area A (and shear areas A_2 and A_3 [8]), as well as to the torsion (J) and bending (I_{22}, I_{33}) inertias, via:

$$\mathbf{C} = EA\mathbf{s}_1 \otimes \mathbf{s}_1 + GA_2\mathbf{s}_2 \otimes \mathbf{s}_2 + GA_3\mathbf{s}_3 \otimes \mathbf{s}_3 \tag{33}$$

$$\mathbf{D} = GJ\mathbf{s}_1 \otimes \mathbf{s}_1 + EI_{33}\mathbf{s}_2 \otimes \mathbf{s}_2 + EI_{22}\mathbf{s}_3 \otimes \mathbf{s}_3 \tag{34}$$

The variation of the sections deformations can be obtained from Eqs. (3) and (4), with help of Eqs. (A4) and (A27), as:

$$\delta\boldsymbol{\Omega} = \mathbf{R}^T \delta\boldsymbol{\theta}' \tag{35}$$

$$\delta\boldsymbol{\Gamma} = \mathbf{R}^T \left(\delta\mathbf{x}' + \mathbf{x}' \times \delta\boldsymbol{\theta} \right) \tag{36}$$

Making use of Eqs. (35) and (36) and integrating by parts, the internal virtual work δU in Eq. (21) can be rewritten as:

$$\delta U = \mathbf{n}\cdot\delta\mathbf{x}\Big|_0^L + \mathbf{m}\cdot\delta\boldsymbol{\theta}\Big|_0^L - \int_0^L \left[\mathbf{n}'\cdot\delta\mathbf{x} + \left(\mathbf{m}' + \mathbf{x}' \times \mathbf{n} \right)\cdot\delta\boldsymbol{\theta} \right] d\xi_1 \tag{37}$$

where the following spatial form of the section resultants is introduced:

$$\mathbf{n} = \mathbf{R}\mathbf{N} \tag{38}$$

$$\mathbf{m} = \mathbf{R}\mathbf{M} \tag{39}$$

Combining Eqs. (19) and (37) and making use of the fundamental lemma of calculus of variations, the following differential equilibrium equations are derived:

$$\mathbf{n}' + \overline{\mathbf{n}} = \mathbf{0} \tag{40}$$

$$\mathbf{m}' + \mathbf{x}' \times \mathbf{n} + \overline{\mathbf{m}} = \mathbf{0} \tag{41}$$

along with the boundary conditions relating the nodal forces and moments to the beam stress-resultants:

$$\mathbf{n}_1 = -\mathbf{n}(0) \tag{42}$$

$$\mathbf{n}_2 = +\mathbf{n}(L) \tag{43}$$

$$\mathbf{m}_1 = -\mathbf{m}(0) \tag{44}$$

$$\mathbf{m}_2 = +\mathbf{m}(L) \tag{45}$$

The kinematic (Eqs. 3 and 4), constitutive (Eqs. 22 - 27) and equilibrium (Eqs. 40 and 41) relations define the beam model. In an usual displacement-based formulation [39, 10, 41] the kinematic fields ($\mathbf{x}$ and $\mathbf{R}$) are interpolated and the section strains ($\boldsymbol{\Gamma}$ and $\boldsymbol{\Omega}$) and resultants ($\mathbf{n}$ and $\mathbf{m}$) are computed as to satisfy the kinematic and constitutive relations exactly but the equilibrium one only in a weak sense. In the present work, an equilibrium-based formulation is proposed. The position $\mathbf{x}$ and rotation $\mathbf{R}$ fields are first interpolated, yielding constant curvature $\boldsymbol{\Omega}_0$ and shear $\boldsymbol{\Gamma}_0$ strains along the beam axis and exactly satisfying the kinematic relation. The stress-resultants $\mathbf{n}$ and $\mathbf{m}$ are then interpolated using the obtained kinematics to exactly satisfy the equilibrium equations. The constitutive relations are solved in a weak sense, determining the equilibrium-based internal variables.

3 | KINEMATICS INTERPOLATION

The interpolation of the position $\mathbf{x}(\xi_1)$ and rotation $\mathbf{R}(\xi_1)$ fields is a key aspect in the development of a TL beam formulation. As mentioned before, Crisfield and Jelenić [10] showed that the interpolation schemes adopted may cause the formulation to lose objectivity and become path-dependent, even when an elastic material response is considered. In this section, non-linear configuration-dependent interpolation functions are adopted for the position and rotation fields. The objectivity and path-independence of the interpolated quantities is verified and the required increments for the tangent stiffness matrix are computed.

Aiming to avoid bending locking, the curvature is set to be constant along the element axis, i.e. $\boldsymbol{\Omega}(\xi_1) = \boldsymbol{\Omega}_0$. Integrating Eq. (3) and applying the boundary condition $\mathbf{R}(0) = \mathbf{R}_1$ at node 1, the rotation field can be expressed as:

$$\mathbf{R}(\xi_1) = \mathbf{R}_1 \exp(\xi_1 \widehat{\boldsymbol{\Omega}}_0) \tag{46}$$

Applying the boundary condition $\mathbf{R}(L) = \mathbf{R}_2$ at node 2, the constant curvature $\boldsymbol{\Omega}_0$ can be determined as a function of the nodal rotations:

$$\widehat{\boldsymbol{\Omega}}_0 = \frac{1}{L} \log\left(\mathbf{R}_1^T \mathbf{R}_2\right) \tag{47}$$

This interpolation of the rotation field is completely equivalent to the one obtained by Crisfield and Jelenić [10] considering the pseudo-vector of the nodes relative rotation. It's interesting to notice the non-linear dependency of the interpolated field $\mathbf{R}(\xi_1)$ on the element current configuration, via the nodal rotation tensors $\mathbf{R}_1$ and $\mathbf{R}_2$. In terms of implementation, to ensure numerical stability and improve performance, the matrix product $\mathbf{R}_1^T\mathbf{R}_2$ in Eq. (47) can be replaced by the unit quaternion product $\mathbf{q}_1^* \circ \mathbf{q}_2$ (where $\mathbf{q}^*$ represents the conjugate quaternion of $\mathbf{q}$), from which the log can be computed by extracting the rotation pseudo-vector [13]. Alternatively, the Spurrier algorithm [30, 37] can be used for the relative rotation tensor.

When a rigid-body motion, with constant rotation $\mathbf{Q}$, is superimposed to the element's current configuration, the curvature becomes:

$$\widehat{\boldsymbol{\Omega}}_0^* = \frac{1}{L} \log\left(\mathbf{R}_1^T \mathbf{Q}^T \mathbf{Q} \mathbf{R}_2\right) = \frac{1}{L} \log\left(\mathbf{R}_1^T \mathbf{R}_2\right) = \widehat{\boldsymbol{\Omega}}_0 \tag{48}$$

Therefore, the interpolation preserves the objectivity of the rotation induced strain measure. Also, the interpolated curvature (Eq. 47) makes reference only to the current values of the nodal rotation tensors, prooving its path-independence. Analogously,

aiming to avoid shear and membrane locking, the translation induced strain is set to be constant along the element axis, i.e. $\boldsymbol{\Gamma}(\xi_1) = \boldsymbol{\Gamma}_0$. With help from Eqs. (A5) and (A14), the following relation can be established:

$$\int_0^{\xi_1} \mathbf{R}(s)ds = \xi_1 \mathbf{R}_1 \mathbf{T}(\xi_1 \widehat{\boldsymbol{\Omega}}_0) \tag{49}$$

Integrating Eq. (4) and applying the boundary condition $\mathbf{x}(0) = \mathbf{x}_1$ at node 1, the position field can be written as:

$$\mathbf{x}(\xi_1) = \mathbf{x}_1 + \xi_1 \mathbf{R}_1 \mathbf{T}(\xi_1 \widehat{\boldsymbol{\Omega}}_0) \left(\mathbf{s}_1 + \boldsymbol{\Gamma}_0\right) \tag{50}$$

Applying the boundary condition $\mathbf{x}(L) = \mathbf{x}_2$ at node 2, the constant translation induced strain $\boldsymbol{\Gamma}_0$ can be written as a function of the nodal configuration:

$$\boldsymbol{\Gamma}_0 = \frac{1}{L}\mathbf{T}^{-1}(L\widehat{\boldsymbol{\Omega}}_0)\mathbf{R}_1^T \left(\mathbf{x}_2 - \mathbf{x}_1\right) \tag{51}$$

The interpolations of the rotation (Eq. 46) and position (Eq. 50) fields are completely equivalent to the ones obtained by Sonneville et al. [40] in the SE(3) space by using the exponential map on the se(3) Lie Algebra. In the present beam formulation, they are simply expressed (and implemented) in the SO(3) and $\mathbb{R}^3$ spaces, respectively, since this spaces are more broadly used in the context of finite elements software and more known to structural engineers then the SE(3) space. It can be seen that both the rotation $\mathbf{R}(\xi_1)$ and position $\mathbf{x}(\xi_1)$ fields depend nonlinearly on the nodal rotations, representing the coupling between the adopted interpolations. When a rigid-body motion, with constant rotation $\mathbf{Q}$ and displacement $\mathbf{c}$, is superimposed to the element's current configuration, the translation induced strain becomes:

$$\begin{aligned}\boldsymbol{\Gamma}_0^* =& \frac{1}{L}\mathbf{T}^{-1}(L\widehat{\boldsymbol{\Omega}}_0)\mathbf{R}_1^T\mathbf{Q}^T \left(\mathbf{Q}\mathbf{x}_2 + \mathbf{c} - \mathbf{Q}\mathbf{x}_1 - \mathbf{c}\right) \\ =& \frac{1}{L}\mathbf{T}^{-1}(L\widehat{\boldsymbol{\Omega}}_0)\mathbf{R}_1^T \left(\mathbf{x}_2 - \mathbf{x}_1\right) = \boldsymbol{\Gamma}_0\end{aligned} \tag{52}$$

Again, the interpolation preserves the objectivity of the translation induced strain measure. Also, the interpolated strain (Eq. 51) makes reference only to the current values of the nodal configuration, prooving its path-independence.

The increments of the section strains ($\Delta\boldsymbol{\Gamma}_0$ and $\Delta\boldsymbol{\Omega}_0$) are necessary to compute the element's tangent stiffness matrix. From Eqs. (47) and (51), we have:

$$\Delta\boldsymbol{\Omega}_0 = \frac{1}{L}\mathbf{T}_0^{-1}\mathbf{R}_1^T \left(\Delta\boldsymbol{\theta}_2 - \Delta\boldsymbol{\theta}_1\right) \tag{53}$$

$$\Delta\boldsymbol{\Gamma}_0 = \frac{1}{L}\mathbf{T}_0^{-1}\mathbf{R}_1^T \left[\Delta\mathbf{x}_2 - \Delta\mathbf{x}_1 + (\mathbf{x}_2 - \mathbf{x}_1)\times\Delta\boldsymbol{\theta}_1\right] + \mathbf{H}_0\mathbf{T}_0^{-1}\mathbf{R}_1^T \left(\Delta\boldsymbol{\theta}_2 - \Delta\boldsymbol{\theta}_1\right) \tag{54}$$

where the following notation has been introduced:

$$\mathbf{T}_0 = \mathbf{T}(L\widehat{\boldsymbol{\Omega}}_0) \tag{55}$$

$$\mathbf{H}_0 = \mathbf{H}[L\widehat{\boldsymbol{\Omega}}_0, \mathbf{R}_1^T \left(\mathbf{x}_2 - \mathbf{x}_1\right)/L] \tag{56}$$

Recalling the relation between the rotation spin vector and the rotation pseudo-vector (Eq. A13), as well as the incremental rotation vector definition at step $n+1$ (Eq. A28), we have:

$$\Delta\boldsymbol{\theta}_k = \mathbf{T}(\widehat{\boldsymbol{\varphi}}_{k,n+1})\Delta\boldsymbol{\varphi}_{k,n+1} \qquad k = 1, 2 \tag{57}$$

It's noteworthy that, the extension of the formulation to high-order interpolations of the strain measures in closed-form can be obtained with special interpolations of the position $\mathbf{x}(\xi_1)$ and rotation $\mathbf{R}(\xi_1)$ fields using a motion approach, as in the displacement-based TL beam formulation developed by Sonneville et al. [42].

4 | EQUILIBRIUM-BASED APPROACH

The Hellinger-Reissner principle, commonly used in mixed beam formulations, makes use of the complementary potential and results, under the action of conservative loads, to strictly symmetric tangent operators. In the developed formulation, there is no underlying mixed principle. Instead, the approach is based on the weak form of the constitutive relations and hence, results is non-symmetric tangent operators (which does not spoil the efficiency of the method). In addition, the section stress-resultants are the outcome of exact integration of the equilibrium equations and not from stress interpolations.

The interpolation of the position $\mathbf{x}$ and rotation $\mathbf{R}$ fields presented in Sec. 3 is now used to obtain the section's resultant forces $\mathbf{n}$ and moments $\mathbf{m}$ in such a way that the equilibrium Eqs. (40) and (41) are satisfied exactly. Integrating along the beam axis, over the interval $[0, \xi_1]$, we obtain:

$$\mathbf{n}(\xi_1) = \mathbf{n}_0 - \int_0^{\xi_1} \overline{\mathbf{n}} d\xi_1 \tag{58}$$

$$\mathbf{m}(\xi_1) = \mathbf{m}_0 + \mathbf{n} \times \left(\mathbf{x} - \mathbf{x}_1\right) - \int_0^{\xi_1} \left[\overline{\mathbf{m}} + \left(\mathbf{x} - \mathbf{x}_1\right) \times \overline{\mathbf{n}}\right] d\xi_1 \tag{59}$$

where $\mathbf{n}_0$ and $\mathbf{m}_0$ are internal parameters to be later determined with the weak form of constitutive relations.

For the sake of simplicity, the distributed forces $\overline{\mathbf{n}}$ and moments $\overline{\mathbf{m}}$ are not considered in the interpolation of the section's resultants. Instead, equivalent nodal quantities are included in the system's external load vector as usual in displacement-based formulations. The resulting interpolated fields are then:

$$\mathbf{n}(\xi_1) = \mathbf{n}_0 \tag{60}$$

$$\mathbf{m}(\xi_1) = \mathbf{m}_0 + \mathbf{n}_0 \times \left(\mathbf{x} - \mathbf{x}_1\right) \tag{61}$$

The interpolated forces $\mathbf{n}$ are then constant over the beam axis. Moreover, considering small curvatures $\boldsymbol{\Omega}_0$, the variation of the interpolated moments $\mathbf{m}$ over the beam axis (given by the term $\mathbf{x} - \mathbf{x}_1$) is approximately linear. This result is also found in CR beam formulations and is a key feature that provides increased accuracy to the present equilibrium-based formulation when compared to traditional displacement-based ones.

Combining Eqs. (31), (32), (38) and (39), the spatial stress-resultants ($\mathbf{n}$ and $\mathbf{m}$) can be related to the section's deformations ($\boldsymbol{\Gamma}$ and $\boldsymbol{\Omega}$). In the exact solution of the beam model, the equilibrium-based form (Eqs. 60 and 61) of the spatial stress-resultants match the one obtained via the constitutive relations. In a equilibrium-based finite element formulation, this condition is satisfied only in a weak sense:

$$\int_0^L (\mathbf{n} - \mathbf{RC}\boldsymbol{\Gamma})\, d\xi_1 = \mathbf{0} \tag{62}$$

$$\int_0^L (\mathbf{m} - \mathbf{RD}\boldsymbol{\Omega})\, d\xi_1 = \mathbf{0} \tag{63}$$

Making use of the rotation field interpolation in Eq. (46) and the equilibrium-based interpolation in Eqs. (60) and (61), the internal parameters $\mathbf{n}_0$ and $\mathbf{m}_0$ can be determined from the weak form of the constitutive relations (Eqs. 62 and 63) as:

$$\mathbf{n}_0 = \mathbf{R}_1 \mathbf{T}_0 \mathbf{C} \boldsymbol{\Gamma}_0 \tag{64}$$

$$\mathbf{m}_0 = \mathbf{R}_1 \mathbf{T}_0 \mathbf{D} \boldsymbol{\Omega}_0 - \mathbf{n}_0 \times \mathbf{x}_0 \tag{65}$$

where:

$$\mathbf{P}_0 = \mathbf{P}(L\widehat{\boldsymbol{\Omega}}_0) \tag{66}$$

$$\mathbf{x}_0 = L\mathbf{R}_1 \mathbf{P}_0 \left(\mathbf{s}_1 + \boldsymbol{\Gamma}_0\right) \tag{67}$$

In Eqs. (64) and (65), the following identities have been used:

$$\mathbf{T}_0 = \frac{1}{L} \int_0^L \exp(\xi_1 \widehat{\boldsymbol{\Omega}}_0) d\xi_1 \tag{68}$$

$$\mathbf{P}_0 = \frac{1}{L^2} \int_0^L \xi_1 \mathbf{T}(\xi_1 \widehat{\boldsymbol{\Omega}}_0) d\xi_1 \tag{69}$$

4.1 | Internal force

From the boundary conditions in Eqs. (42 - 45), the nodal forces ($\mathbf{n}_1$ and $\mathbf{n}_2$) and the nodal moments ($\mathbf{m}_1$ and $\mathbf{m}_2$), representing the element internal force vector $\mathbf{f}$, can be simply obtained as:

$$\mathbf{f} = \begin{Bmatrix} \mathbf{n}_1 \\ \mathbf{m}_1 \\ \mathbf{n}_2 \\ \mathbf{m}_2 \end{Bmatrix} = \begin{Bmatrix} -\mathbf{n}_0 \\ -\mathbf{m}_0 \\ +\mathbf{n}_0 \\ \mathbf{m}_0 + \mathbf{n}_0 \times \left(\mathbf{x}_2 - \mathbf{x}_1\right) \end{Bmatrix} \tag{70}$$

It's noteworthy that, due to the construction of kinematic configuration-dependent interpolations with constant deformations $\boldsymbol{\Gamma}_0$ and $\boldsymbol{\Omega}_0$, the integral over the beam axis can be computed explicitly, and so no numerical integration scheme needs to be employed. This has a significant impact on the efficiency of the numerical formulation, considerably reducing the computational cost.

It's also easy to show that the obtained internal force vector $\mathbf{f}$ exactly satisfies the equilibrium of an isolated element:

$$\mathbf{n}_1 + \mathbf{n}_2 = \mathbf{0} \tag{71}$$

$$\mathbf{m}_1 + \mathbf{m}_2 + (\mathbf{x}_2 - \mathbf{x}_1) \times \mathbf{n}_2 = \mathbf{0} \tag{72}$$

Therefore, even in the non-converged iterations of the incremental-iterative solution procedure the element is self-equilibrated. This is an important property of a finite element formulation, increasing its accuracy and convergence rate, as demonstrated by [23, 25].

4.2 | Tangent Stiffness

The element's tangent stiffness matrix $\mathbf{K}$ is now computed by taking the increment of the internal force vector $\Delta\mathbf{f}$ with respect to the nodal degrees of freedom $\Delta\mathbf{d}$, that is:

$$\Delta\mathbf{f} = \mathbf{K}\Delta\mathbf{d} = \begin{bmatrix} \mathbf{K}_{11} & \mathbf{K}_{12} & \mathbf{K}_{13} & \mathbf{K}_{14} \\ \mathbf{K}_{21} & \mathbf{K}_{22} & \mathbf{K}_{23} & \mathbf{K}_{24} \\ \mathbf{K}_{31} & \mathbf{K}_{32} & \mathbf{K}_{33} & \mathbf{K}_{34} \\ \mathbf{K}_{41} & \mathbf{K}_{42} & \mathbf{K}_{43} & \mathbf{K}_{44} \end{bmatrix} \begin{Bmatrix} \Delta\mathbf{x}_1 \\ \Delta\boldsymbol{\theta}_1 \\ \Delta\mathbf{x}_2 \\ \Delta\boldsymbol{\theta}_2 \end{Bmatrix} \tag{73}$$

From equilibrium considerations (Eqs. 71 and 72), the following relations can be obtained:

$$\mathbf{K}_{31} = -\mathbf{K}_{11} \tag{74}$$

$$\mathbf{K}_{32} = -\mathbf{K}_{12} \tag{75}$$

$$\mathbf{K}_{33} = -\mathbf{K}_{13} \tag{76}$$

$$\mathbf{K}_{34} = -\mathbf{K}_{14} \tag{77}$$

$$\mathbf{K}_{42} = -\mathbf{K}_{22} + \left(\widehat{\mathbf{x}}_2 - \widehat{\mathbf{x}}_1\right)\mathbf{K}_{12} \tag{78}$$

$$\mathbf{K}_{44} = -\mathbf{K}_{24} + \left(\widehat{\mathbf{x}}_2 - \widehat{\mathbf{x}}_1\right)\mathbf{K}_{14} \tag{79}$$

$$\mathbf{K}_{41} = -\mathbf{K}_{21} + \left(\widehat{\mathbf{x}}_2 - \widehat{\mathbf{x}}_1\right)\mathbf{K}_{11} + \widehat{\mathbf{n}}_1 \tag{80}$$

$$\mathbf{K}_{43} = -\mathbf{K}_{23} + \left(\widehat{\mathbf{x}}_2 - \widehat{\mathbf{x}}_1\right)\mathbf{K}_{13} - \widehat{\mathbf{n}}_1 \tag{81}$$

The remaining terms of the tangent stiffness matrix $\mathbf{K}$ are obtained by taking the increment of the internal parameters $\mathbf{n}_0$ and $\mathbf{m}_0$ in Eqs. (64) and (65). With help of Eqs. (53), (54) and (A24), after some lengthy but otherwise straight-forward calculations, we obtain:

$$\mathbf{K}_{11} = +\frac{1}{L}\mathbf{R}_1\mathbf{T}_0\mathbf{C}\mathbf{T}_0^{-1}\mathbf{R}_1^T \tag{82}$$

$$\mathbf{K}_{13} = -\frac{1}{L}\mathbf{R}_1\mathbf{T}_0\mathbf{C}\mathbf{T}_0^{-1}\mathbf{R}_1^T \tag{83}$$

$$\mathbf{K}_{14} = -\mathbf{R}_1(\mathbf{G}_c + \mathbf{T}_0\mathbf{C}\mathbf{H}_0)\mathbf{T}_0^{-1}\mathbf{R}_1^T \tag{84}$$

$$\mathbf{K}_{21} = +L\widehat{\mathbf{x}}_0\mathbf{K}_{11} - \widehat{\mathbf{n}}_0\mathbf{R}_1\mathbf{P}_0\mathbf{T}_0^{-1}\mathbf{R}_1^T \tag{85}$$

$$\mathbf{K}_{23} = +L\hat{\mathbf{x}}_0\mathbf{K}_{13} + \hat{\mathbf{n}}_0\mathbf{R}_1\mathbf{P}_0\mathbf{T}_0^{-1}\mathbf{R}_1^T \tag{86}$$

$$\mathbf{K}_{12} = +\mathbf{R}_1(\mathbf{G}_c + \mathbf{T}_0\mathbf{C}\mathbf{H}_0)\mathbf{T}_0^{-1}\mathbf{R}_1^T - \frac{1}{L}\mathbf{R}_1\mathbf{T}_0\mathbf{C}\mathbf{T}_0^{-1}\mathbf{R}_1^T(\hat{\mathbf{x}}_2 - \hat{\mathbf{x}}_1) + \hat{\mathbf{n}}_0 \tag{87}$$

$$\mathbf{K}_{24} = -\left[\mathbf{R}_1\left(\mathbf{G}_d + \frac{1}{L}\mathbf{T}_0\mathbf{D}\right) + L\hat{\mathbf{n}}_0\mathbf{R}_1\left(\mathbf{Q}_0 + \mathbf{P}_0\mathbf{H}_0\right)\right]\mathbf{T}_0^{-1}\mathbf{R}_1^T + \hat{\mathbf{x}}_0\mathbf{K}_{14} \tag{88}$$

$$\mathbf{K}_{22} = +\left[\mathbf{R}_1\left(\mathbf{G}_d + \frac{1}{L}\mathbf{T}_0\mathbf{D}\right) + L\hat{\mathbf{n}}_0\mathbf{R}_1\left(\mathbf{Q}_0 + \mathbf{P}_0\mathbf{H}_0\right)\right]\mathbf{T}_0^{-1}\mathbf{R}_1^T + \hat{\mathbf{x}}_0\mathbf{K}_{12} + \text{skew}(\mathbf{R}_1\mathbf{T}_0\mathbf{D}\boldsymbol{\Omega}_0) - \hat{\mathbf{n}}_0\hat{\mathbf{x}}_0 + \hat{\mathbf{n}}_0\mathbf{R}_1\mathbf{P}_0\mathbf{T}_0^{-1}\mathbf{R}_1^T(\hat{\mathbf{x}}_2 - \hat{\mathbf{x}}_1) \tag{89}$$

where:

$$\mathbf{G}_d = \mathbf{G}(L\hat{\boldsymbol{\Omega}}_0, \mathbf{D}\boldsymbol{\Omega}_0) \tag{90}$$

$$\mathbf{G}_c = \mathbf{G}(L\hat{\boldsymbol{\Omega}}_0, \mathbf{C}\boldsymbol{\Gamma}_0) \tag{91}$$

$$\mathbf{Q}_0 = \mathbf{Q}(L\hat{\boldsymbol{\Omega}}_0, \mathbf{s}_1 + \boldsymbol{\Gamma}_0) \tag{92}$$

It's noteworthy that, since the present formulation is not based in an energy principal, the tangent stiffness matrix is not symmetric. However, as closed-form expressions are obtained for the internal force vector and the tangent stiffness matrix, they can be computed explicitly (without numerical integration), considerably reducing the computational cost and so yielding a highly efficient finite element formulation.

5 | NUMERICAL APPLICATIONS

The developed formulation has been implemented in the non-linear finite element software GALILEO [32]. In this section, a number of structural systems are modeled with the proposed beam element in order to assess its accuracy, performance and convergence properties. First, the absence of locking is verified. Then, the formulation accuracy and performance is tested analyzing systems with strong non-linear response.

5.1 | Clamped beam

The first example consists of a fully clamped beam made of steel with Poisson's ratio $\nu = 0.3$ and elastic modulus $E = 200$ GPa. The beam has a span of $L = 4$ m and is subjected to a mid-span transverse force $P = 42.9$ MN (Fig. 2), designed to cause a mid-span vertical displacement equal to 10% of the beam's span, introducing large displacements and rotations. The beam has a hollow rectangular cross-section 20 cm wide by 40 cm deep and 6 mm thickness. The displacements and rotations at both ends are fixed in order to maximize the shear deformations and so demonstrate the formulation's absence of shear-locking.

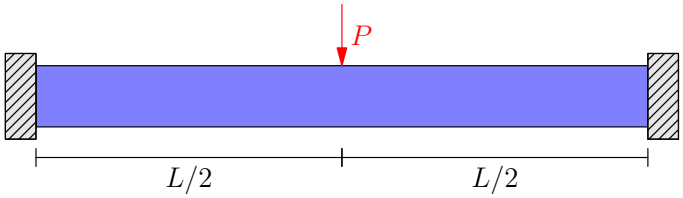

FIGURE 2 Clamped beam subjected to a mid-span transverse force.

The convergence analysis with the present formulation is shown in Fig. 3. With only five elements, the relative error is of 2.00%, highlighting the fast convergence and absence of the shear locking in the formulation. This property is directly related to the adopted configuration-dependent interpolation functions, as shown in [40]. In fact, the convergence analysis with the displacement-based version of the present formulation, developed by Sonneville et al. [41], yields very close results. The main advantage of the present formulation is the gain in accuracy of the computed section stress-resultants for coarse meshes, as can be seen in Fig. 4, where the shear force and bending moment diagrams of the displacement-based [41] and equilibrium-based formulations with 5 elements are compared to the converged solution (100 elements).

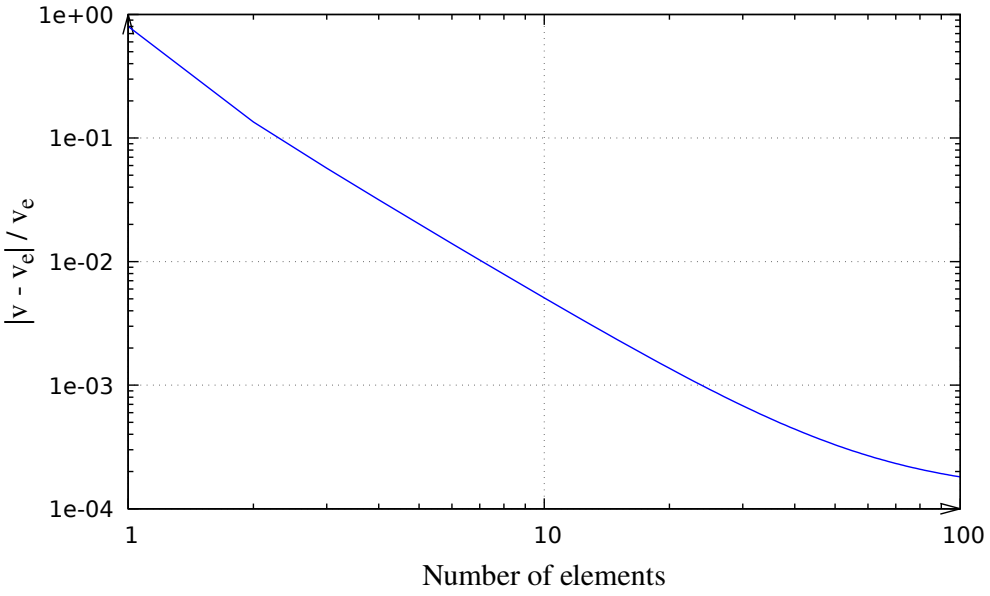

FIGURE 3 Convergence analysis of the clamped beam subjected to mid-span transverse force.

5.2 | Cantilever beam bending

The next example consists of a cantilever beam subjected to an tip bending moment $M = 2\pi\lambda EI/L$ (Fig. 2). At full loading ($\lambda = 1$), the beam folds into a circle ($\psi = 2\pi$). The exact solution to this problem [26] provides null shear deformations. However, as discussed in [41], the finite element formulation of shear deformable beams with linear interpolation and exact spatial integration exhibits a shear-locking phenomenon [39]. With the developed formulation, the shear strains of the beam finite element are identically zero. Moreover, since in this problem the bending deformation is constant along the element, the exact solution can be obtained with a single element.

For the numerical analysis, the beam has a hollow rectangular cross-section 20 cm wide by 40 cm deep and 6 mm thickness. The beam has a span of $L = 4$ m and is made of steel with Poisson's ratio $\nu = 0.3$ and elastic modulus $E = 200$ GPa. The obtained results are shown in Fig. 6, where the loaded end horizontal u and vertical v displacements with a single element of the developed formulation exactly matches the closed-form solution [26].

5.3 | L frame

The next example consists of a cantilever L-shaped frame subjected to a end force P (Fig. 7). The beam has a rectangular section with 0.6 cm wide by 30 cm deep. The beam has a span of $L = 240$ cm and is made of a material with Poisson's ratio $\nu = 0.31$ and elastic modulus $E = 71.24$ GPa. This classical benchmark has been studied by a number of authors, including [4, 9, 39]. Although the geometry and boundary conditions of the problem are planar, due to the small torsional stiffness associated with the thin section, the frame buckles out of plane.

The variation of the out-of-plane displacement w of the tip node with the applied load P are shown in Fig. 8. Battini and Pacoste [4] discretized each beam in ten finite elements. In the present work, only four finite elements are used per member and a good agreement between the results can be observed.

5.4 | Deployable ring

The next example consists of the deployable ring shown in Fig. 9. The ring has a rectangular section 0.6 mm wide and 6 cm deep, with radius $R = 120$ mm. The ring is made of a material with Poisson's ratio $\nu = 0.3$ and elastic modulus $E = 200$ GPa. The system is subjected to a torsion moment M at point A, where it's also constrained to move and rotate in the x direction. At point B the displacements and rotations are fixed.

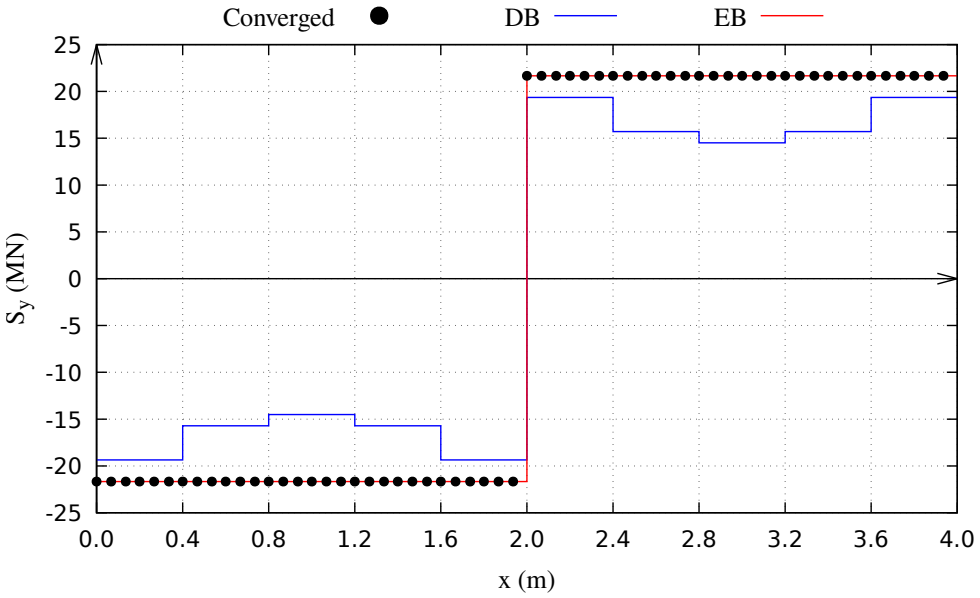

(a) Shear force diagram

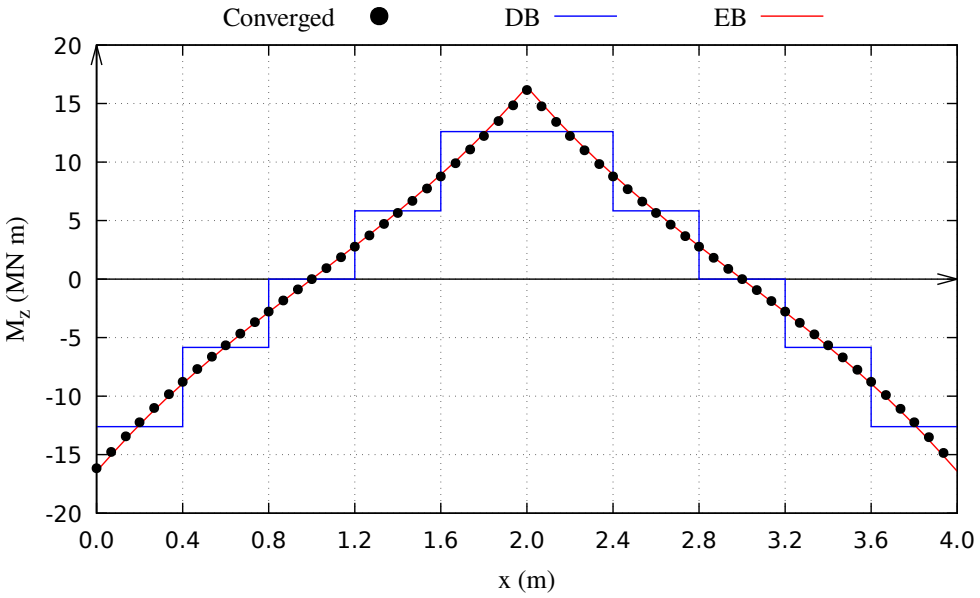

(b) Bending moment diagram

FIGURE 4 Section stress-resultants of the clamped beam with displacement-based (DB) and equilibrium-based (EB) formulations.

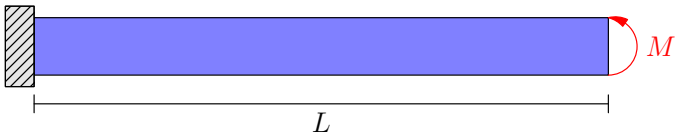

FIGURE 5 Cantilever beam subjected to a tip bending moment.

This benchmark was introduced by [14] and also studied by [4]. After a complete rotation about point A ($\psi_A = 2\pi$), the ring folds around itself, transforming in a smaller ring with a third of the original radius. After another complete rotation ($\psi_A = 4\pi$), the ring returns to the original configuration.

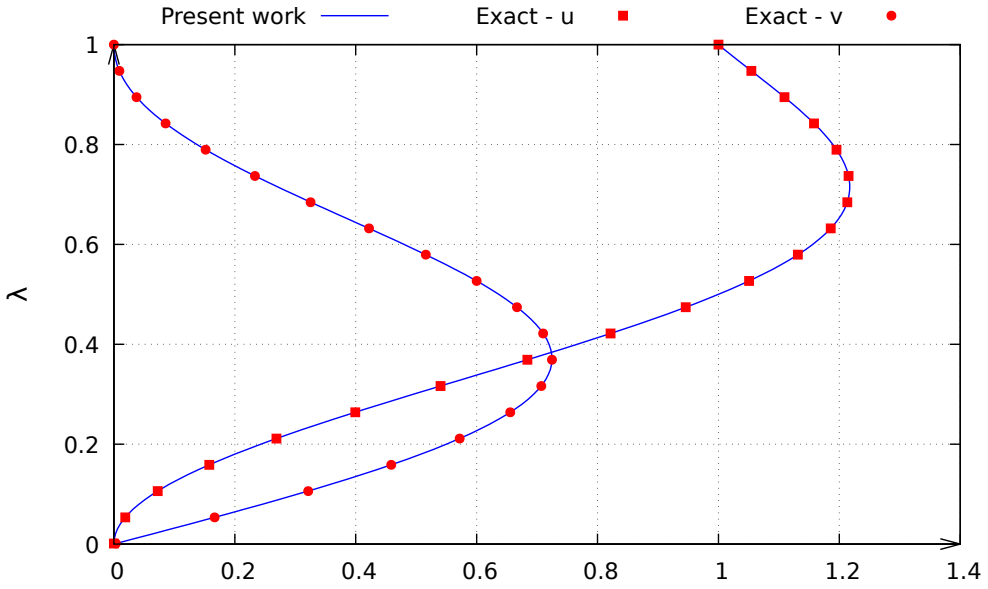

FIGURE 6 Equilibrium path of the cantilever beam subjected to tip bending moment.

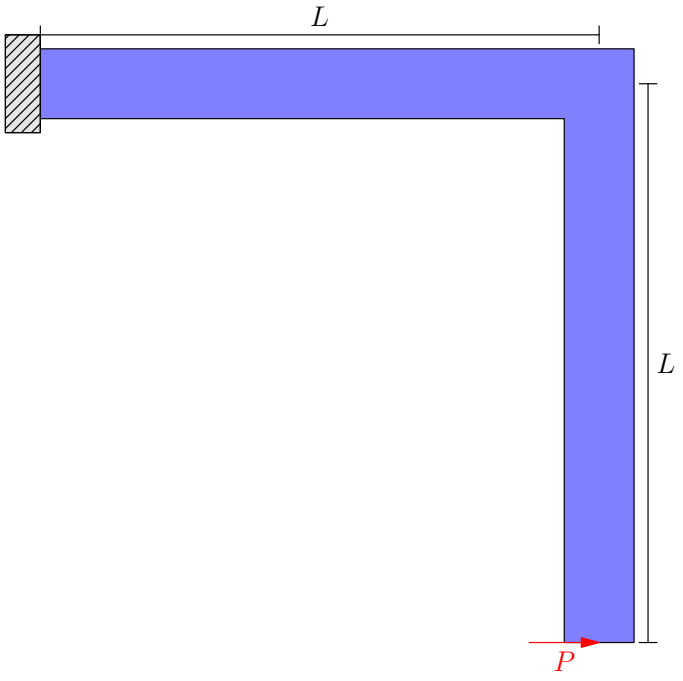

FIGURE 7 L-shaped frame subjected to a tip force.

In order to accurately represent the geometry of the reference configuration, a mesh with 128 finite elements are used. The obtained results are shown in Fig. 10 and presents a successful match when compared with [4].

For the numerical analysis, 650 load steps were used with a load increment $\Delta M = 1$ N m. The total CPU time with the formulation proposed by [41] and the developed formulation were 18.40 s and 14.03 s, respectively, representing a gain of 23.75% in performance.

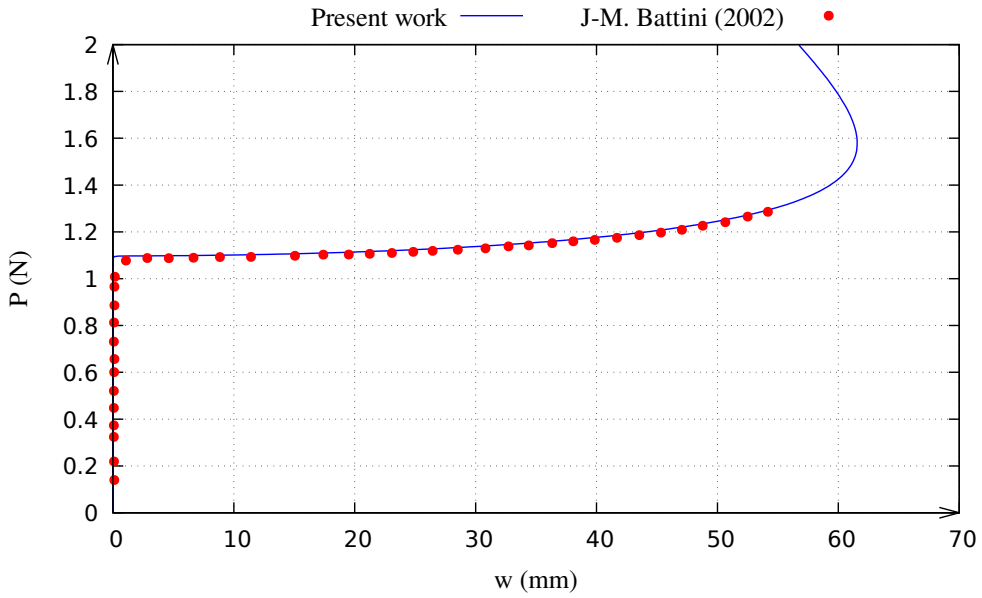

FIGURE 8 Equilibrium path of the L-shaped frame subjected to a tip force.

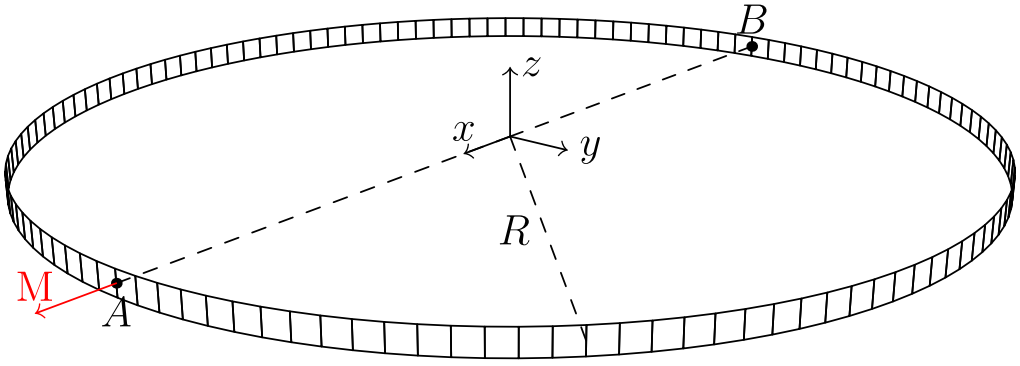

FIGURE 9 Deployable ring subjected to a torsion moment.

5.5 | Framed dome

The last example consists of the framed dome shown in Fig. 11. This model was first introduced by [16] and also studied by [4]. The dome's beams have a rectangular cross-section with 0.76 wide by 1.22 deep and are made of a material with Poisson's ratio $\nu = 0.17$ and elastic modulus $E = 20690$. The dome's geometry is determined with the parameters $r_1 = 12.57$, $r_2 = 24.38$, $h_1 = 4.55$ and $h_2 = 1.55$.

In the numerical analysis, each beam is discretized in $n_b = 5$ finite elements and so the mesh contained a total of $n_e = 90$ finite elements. Initially, the primary path (PP) is computed with the load P applied perfectly centered at the apex node. Then, in a second simulation, a small geometric imperfection is added to the apex node coordinates, in order to induce the secondary path (SP) with a rotational buckling mode (Fig. 12). The obtained results are shown in Fig. 13 and presents a successful match when compared with [4].

For the numerical analysis, 800 load steps were used with a load increment $\Delta P = 2$. The total CPU time with the formulation proposed by [4] and the developed formulation were 10.10 s and 7.86 s, respectively, representing a gain of 22.16% in performance. Also, in avarage, 2.72 iterations were required per load step to achive equilibrium with the formulation proposed in [4], while only 1.10 iterations were necessary with the developed formulation.

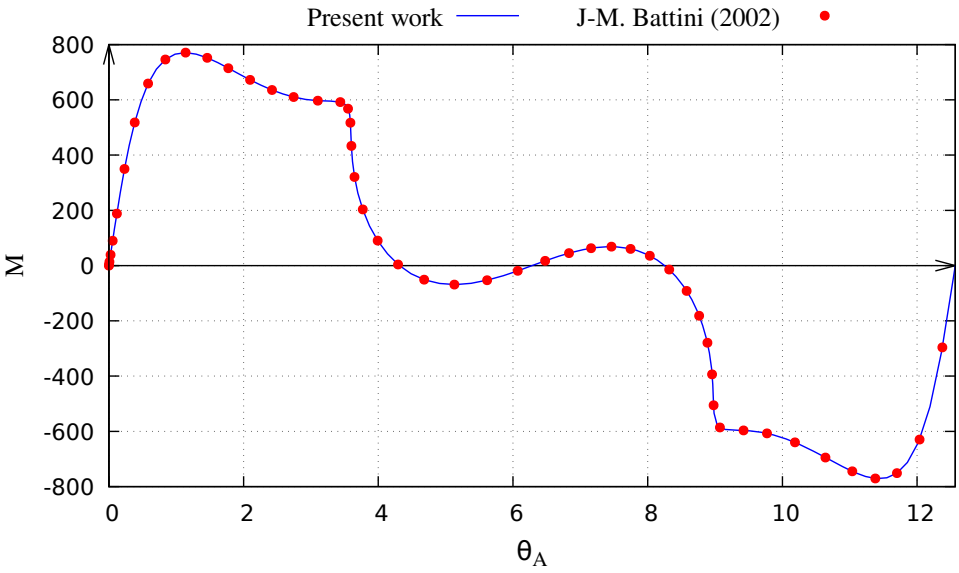

FIGURE 10 Equilibrium path of the deployable ring subjected to a torsion moment.

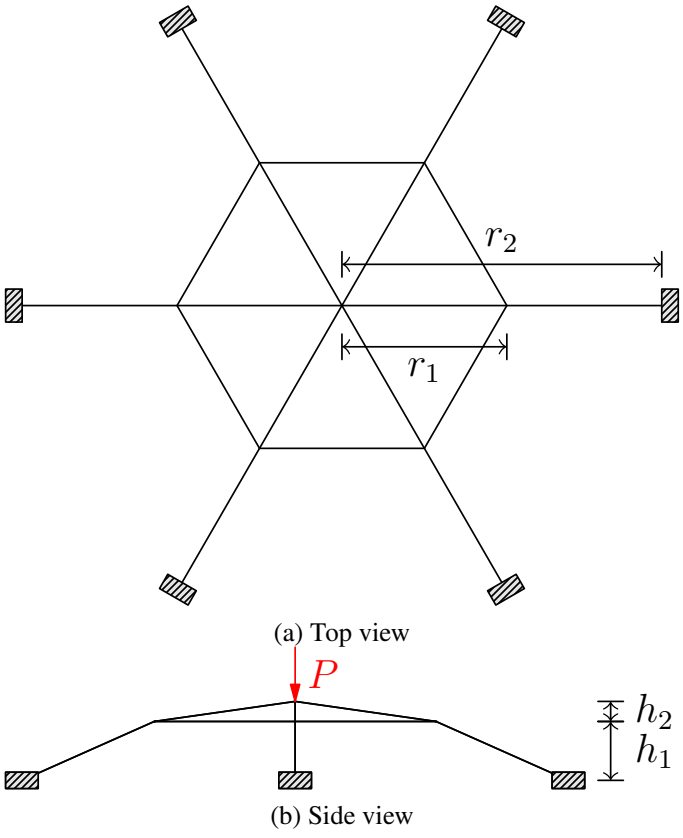

FIGURE 11 Framed dome subjected to a force.

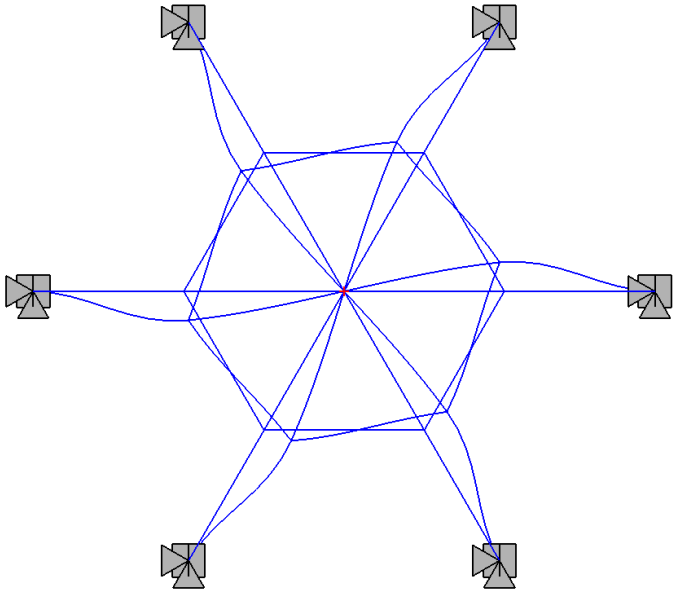

FIGURE 12 Buckling mode of the framed dome subjected to a force.

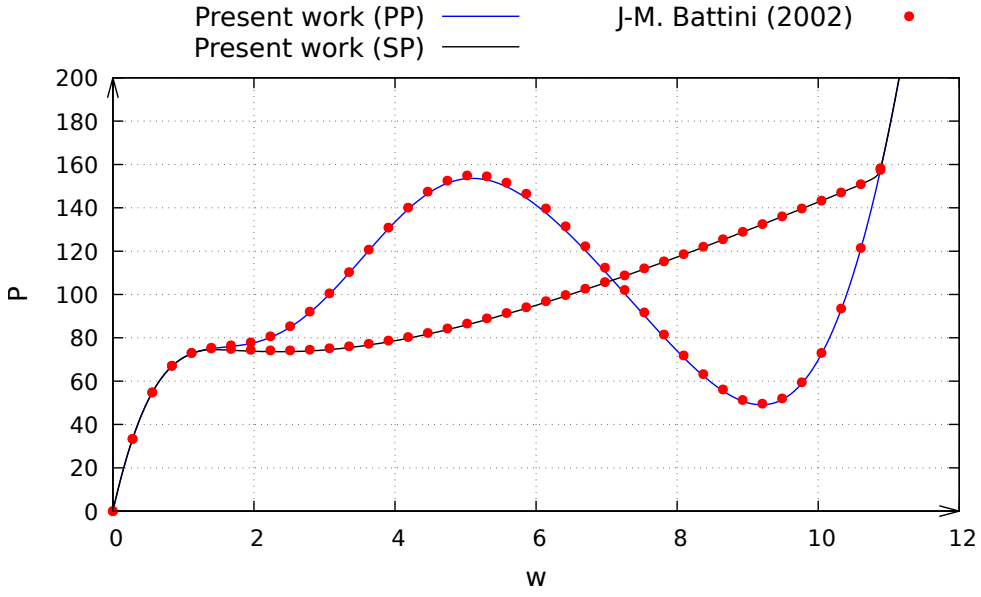

FIGURE 13 Equilibrium path of the framed dome subjected to a force.

6 | CONCLUSIONS

The present work addresses the formulation of a novel equilibrium-based geometrically-exact TL beam finite element. The first step is to obtain non-linear configuration-dependent interpolation of the position and rotation fields by enforcing constant translation and rotation induced section strains. Next, the resulting kinematic fields are used to construct equilibrium-based interpolation for the stress-resultant fields, that exactly satisfies the equilibrium equations. The obtained internal force vector and tangent stiffness matrix are self-equilibrated and computed via closed-form expressions. As a result, no numerical integration is required, yielding a computationally efficient numerical method. The formulation is successfully tested with respect to classical

strongly non-linear structural systems. The developed formulation shows improved accuracy and convergence rate when compared to existing formulations in the literature. It's also shown that the closed-form expressions obtained for the internal force vector and tangent stiffness considerably reduce the required computational time.

Non-uniform torsion deformations are important when studying beams with thin-walled profiles and can be included in the finite element formulation by adopting the Vlasov's beam theory. With this modification, the assumption of rigid section motion is relaxed and warping deformation modes appear, together with additional stress-resultants, namely the bi-shear and bi-moment. Also, the formulation can be adapted to take into account curved initial configurations, as in the displacement-based TL beam formulation developed by Sonneville et al. [42]. The main change is that the initial cross-section triads varies along the beam axis and so, the simple stress constitutive relations in Eqs. (28) - (30) are no longer valid. Instead, more elaborate relations are need, which take into account the initial curvatures and extensions. For this, the curvilinear co-variant and contra-variant directions are used, influencing the weak form of the section stress-resultants constitutive relations (Eqs. 62 and 63).

The elasto-plastic material behavior could be considered while computing the section stress-resultants in Eqs. (22) - (27). In this case, integration over the section domain must be performed taking into account the history of deformation. However, due to the adopted configuration-dependent interpolation of the kinematic fields, explicit integration over the beam axis can still be achieved, maintaining the formulation performance. Finally, the proposed interpolation of the position and rotation fields introduces a new kinematics from which the mass matrix and inertia forces can be obtained for a complete dynamic non-linear analysis [40].

ACKNOWLEDGEMENTS

The authors gratefully acknowledge financial support by the Walloon Region of Belgium and bureau d'études Greisch through the research grant n°8096, "FINELG2020".

□

APPENDIX

A SPATIAL ROTATIONS

In this appendix, the standard relations for spatial rotations are presented for completeness. The rotation tensor $\mathbf{R}$ is an element of the special orthogonal group SO(3), that is:

$$\det(\mathbf{R}) = 1 \tag{A1}$$

$$\mathbf{R}^T\mathbf{R} = \mathbf{R}\mathbf{R}^T = \mathbf{I} \tag{A2}$$

where $\mathbf{I}$ represents the 3×3 identity matrix. Taking the variation of Eq. (A2) we obtain:

$$\delta\mathbf{R}\mathbf{R}^T = -\left(\delta\mathbf{R}\mathbf{R}^T\right)^T \tag{A3}$$

The product $\delta\mathbf{R}\mathbf{R}^T$ is then skew-symmetric and for some vector $\delta\boldsymbol{\theta}$, we have:

$$\delta\mathbf{R} = \delta\widehat{\boldsymbol{\theta}}\mathbf{R} \tag{A4}$$

where $\delta\widehat{\boldsymbol{\theta}}$ represents the skew-symmetric matrix obtained from the rotation spin vector $\delta\boldsymbol{\theta}$. This shows that the set of 3×3 skew-symmetric matrices so(3) forms the Lie Algebra of to the Lie Group SO(3). The rotation tensor can then be parameterized by a rotation pseudo-vector $\boldsymbol{\varphi}$ via the exponential map:

$$\mathbf{R}(\widehat{\boldsymbol{\varphi}}) = \exp(\widehat{\boldsymbol{\varphi}}) = \sum_{k=0}^{\infty} \frac{\widehat{\boldsymbol{\varphi}}^k}{k!} \tag{A5}$$

The square of a skew-matrix $\widehat{\boldsymbol{\varphi}}^2$ can be related to the outer product $\boldsymbol{\varphi} \otimes \boldsymbol{\varphi}$ and the identity matrix $\mathbf{I}$ as:

$$\widehat{\boldsymbol{\varphi}}^2 = \boldsymbol{\varphi} \otimes \boldsymbol{\varphi} - \varphi^2\mathbf{I} \tag{A6}$$

where $\varphi = \sqrt{\boldsymbol{\varphi} \cdot \boldsymbol{\varphi}}$.

The following identities then hold for any $k \in \mathbb{Z}$:

$$\widehat{\boldsymbol{\varphi}}^{2k+1} = (-1)^k \varphi^{2k} \widehat{\boldsymbol{\varphi}} \tag{A7}$$

$$\widehat{\boldsymbol{\varphi}}^{2k+2} = (-1)^k \varphi^{2k} \widehat{\boldsymbol{\varphi}}^2 \tag{A8}$$

Here, the class of functions $f_n : \mathbb{R} \to \mathbb{R}$ is introduced as:

$$f_n(\varphi) = \sum_{k=0}^{\infty} \frac{(-1)^k \varphi^{2k}}{(2k+n)!} \tag{A9}$$

Combining Eqs. (A5), (A7), (A8) and (A9), the rotation tensor can be written in the form:

$$\mathbf{R}(\widehat{\boldsymbol{\varphi}}) = \mathbf{I} + f_1(\varphi)\widehat{\boldsymbol{\varphi}} + f_2(\varphi)\widehat{\boldsymbol{\varphi}}^2 \tag{A10}$$

Recalling the series expansion of the cos and sin functions, the infinite series in Eq. (A9) can be replaced with:

$$f_n(\varphi) = \begin{cases} \frac{(-1)^p}{\varphi^n} \left[\cos(\varphi) - \sum_{k=0}^{p-1} \frac{(-1)^k \varphi^{2k}}{(2k)!} \right] & \text{if } n = 2p \\ \frac{(-1)^p}{\varphi^n} \left[\sin(\varphi) - \sum_{k=0}^{p-1} \frac{(-1)^k \varphi^{2k+1}}{(2k+1)!} \right] & \text{if } n = 2p+1 \end{cases} \tag{A11}$$

In practice, the form in Eq. (A9) is more numerically stable for small angles (say $|\varphi| < 2\pi$) and only a few terms need to be considered, whereas the form in Eq. (A11) is more numerically stable for larger angles. By mathematical induction, it can be shown that the derivatives of the rotation class function are computed as:

$$f_n'(\varphi) = \varphi \left[n f_{n+2}(\varphi) - f_{n+1}(\varphi) \right] \tag{A12}$$

Combining Eq. (A4) with the variation of Eq. (A10), the rotation spin vector $\delta\boldsymbol{\theta}$ can be related to the variation of the rotation pseudo-vector $\delta\boldsymbol{\varphi}$ as:

$$\delta\boldsymbol{\theta} = \mathbf{T}(\widehat{\boldsymbol{\varphi}})\delta\boldsymbol{\varphi} \tag{A13}$$

where the rotation gradient $\mathbf{T}(\widehat{\boldsymbol{\varphi}})$ is given by:

$$\mathbf{T}(\widehat{\boldsymbol{\varphi}}) = \sum_{k=0}^{\infty} \frac{\widehat{\boldsymbol{\varphi}}^k}{(k+1)!} = \mathbf{I} + f_2(\varphi)\widehat{\boldsymbol{\varphi}} + f_3(\varphi)\widehat{\boldsymbol{\varphi}}^2 \tag{A14}$$

The variation of the rotation gradient $\mathbf{T}(\widehat{\boldsymbol{\varphi}})$ with respect to the pseudo-vector $\boldsymbol{\varphi}$ can be written as:

$$\delta\mathbf{T}(\widehat{\boldsymbol{\varphi}})\mathbf{v} = \mathbf{G}(\widehat{\boldsymbol{\varphi}}, \mathbf{v})\delta\boldsymbol{\varphi} \quad \forall \mathbf{v} \in \mathbb{R}^3 \tag{A15}$$

with the rotation hessian $\mathbf{G}(\widehat{\boldsymbol{\varphi}}, \mathbf{v})$ being defined as:

$$\begin{aligned} \mathbf{G}(\widehat{\boldsymbol{\varphi}}, \mathbf{v}) = & \frac{1}{\varphi} \left[f_2'(\varphi)\boldsymbol{\varphi} \times \mathbf{v} + f_3'(\varphi)\boldsymbol{\varphi} \times (\boldsymbol{\varphi} \times \mathbf{v}) \right] \otimes \boldsymbol{\varphi} - \\ & f_2(\varphi)\widehat{\mathbf{v}} - f_3(\varphi) \left(2\widehat{\boldsymbol{\varphi}}\widehat{\mathbf{v}} - \widehat{\mathbf{v}}\widehat{\boldsymbol{\varphi}} \right) \end{aligned} \tag{A16}$$

The rotation gradient inverse can also be obtained as [17]:

$$\mathbf{T}^{-1}(\widehat{\boldsymbol{\varphi}}) = \mathbf{I} - \frac{1}{2}\widehat{\boldsymbol{\varphi}} + \frac{f_3(\varphi) - 2f_4(\varphi)}{2f_2(\varphi)}\widehat{\boldsymbol{\varphi}}^2 \tag{A17}$$

The variation of the rotation gradient inverse $\mathbf{T}^{-1}(\widehat{\boldsymbol{\varphi}})$ with respect to the pseudo-vector $\boldsymbol{\varphi}$ can be written as:

$$\delta\mathbf{T}^{-1}(\widehat{\boldsymbol{\varphi}})\mathbf{v} = \mathbf{H}(\widehat{\boldsymbol{\varphi}}, \mathbf{v})\delta\boldsymbol{\varphi} \quad \forall \mathbf{v} \in \mathbb{R}^3 \tag{A18}$$

with the rotation hessian inverse $\mathbf{H}(\widehat{\boldsymbol{\varphi}}, \mathbf{v})$ being defined as:

$$\mathbf{H}(\widehat{\boldsymbol{\varphi}}, \mathbf{v}) = \frac{1}{2}\widehat{\mathbf{v}} + a(\widehat{\mathbf{v}}\widehat{\boldsymbol{\varphi}} - 2\widehat{\boldsymbol{\varphi}}\widehat{\mathbf{v}}) + b\left[\boldsymbol{\varphi} \times (\boldsymbol{\varphi} \times \mathbf{v})\right] \otimes \boldsymbol{\varphi} \tag{A19}$$

where:

$$a = \frac{f_3(\varphi) - 2f_4(\varphi)}{2f_2(\varphi)} \tag{A20}$$

$$b = \frac{f_5(\varphi) - 4f_6(\varphi)}{2f_2(\varphi)} \tag{A21}$$

The second order gradient $\mathbf{P}(\widehat{\boldsymbol{\varphi}})$ is introduced here as:

$$\mathbf{P}(\widehat{\boldsymbol{\varphi}}) = \sum_{k=0}^{\infty} \frac{\widehat{\boldsymbol{\varphi}}^k}{(k+2)!} = f_2(0)\mathbf{I} + f_3(\varphi)\widehat{\boldsymbol{\varphi}} + f_4(\varphi)\widehat{\boldsymbol{\varphi}}^2 \tag{A22}$$

The variation of the tensor $\mathbf{P}(\boldsymbol{\varphi})$ with respect to the pseudo-vector $\boldsymbol{\varphi}$ can be written as:

$$\delta\mathbf{P}(\widehat{\boldsymbol{\varphi}})\mathbf{v} = \mathbf{Q}(\boldsymbol{\varphi}, \mathbf{v})\delta\boldsymbol{\varphi} \quad \forall \mathbf{v} \in \mathbb{R}^3 \tag{A23}$$

where:

$$\mathbf{Q}(\widehat{\boldsymbol{\varphi}}, \mathbf{v}) = \frac{1}{\varphi}\left[f_3'(\varphi)\widehat{\boldsymbol{\varphi}}\mathbf{v} + f_4'(\varphi)\widehat{\boldsymbol{\varphi}}^2\mathbf{v}\right] \otimes \boldsymbol{\varphi} - f_3(\varphi)\widehat{\mathbf{v}} - f_4(\varphi)\left(2\widehat{\boldsymbol{\varphi}}\widehat{\mathbf{v}} - \widehat{\mathbf{v}}\widehat{\boldsymbol{\varphi}}\right) \tag{A24}$$

If the rotation tensor $\mathbf{R}$ is a function of some spatial coordinate ξ_1, the derivative of Eq. (A2) provides:

$$\mathbf{R}^T\mathbf{R}' = -\left(\mathbf{R}^T\mathbf{R}'\right) \tag{A25}$$

The product $\mathbf{R}^T\mathbf{R}'$ is then skew-symmetric and for some curvature vector $\boldsymbol{\Omega}$, we have:

$$\mathbf{R}' = \mathbf{R}\widehat{\boldsymbol{\Omega}} \tag{A26}$$

Combining the derivative of Eq. (A4) and the increment of Eq. (A26), the following relation between the curvature increment $\Delta\boldsymbol{\Omega}$ and rotation spin derivative $\Delta\boldsymbol{\theta}'$ can be obtained:

$$\Delta\boldsymbol{\Omega} = \mathbf{R}^T\Delta\boldsymbol{\theta}' \tag{A27}$$

As $\det(\mathbf{T}) = 2f_2(\varphi)$, the relation in Eq. (A14) becomes singular when $\varphi = 2\pi k$, with $k \in \mathbb{N}$. In a finite element analysis this makes the stiffness matrix ill-conditioned, causing the iterative procedure to fail. The total rotation pseudo-vector is then limited to the interval $\varphi \in [0, 2\pi)$. To circumvent this issue, the incremental rotation pseudo-vector is used to parameterize the rotation tensor. In a incremental solution procedure, the rotation tensor $\mathbf{R}_n$ at step n is stored and at step $n+1$, we have:

$$\mathbf{R}_{n+1} = \exp(\widehat{\boldsymbol{\varphi}}_{n+1})\mathbf{R}_n \tag{A28}$$

The update procedure can become more robust and memory efficient by working with the quaternion version of Eq. (A28):

$$\mathbf{q}_{n+1} = \mathrm{quat}(\boldsymbol{\varphi}_{n+1}) \circ \mathbf{q}_n \tag{A29}$$

where quat represents the function that computes the quaternion from a given rotation pseudo-vector and $\circ$ is the quaternion product [37].

References

[1] R. Alsafadie, M. Hjiaj, and J.-M. Battini. Three-dimensional formulation of a mixed corotational thin-walled beam element incorporating shear and warping deformation. *Thin-Walled Structures*, 49(4):523–533, Apr. 2011.

[2] M. M. Attard. Finite strain—beam theory. *International Journal of Solids and Structures*, 40(17):4563–4584, Aug. 2003.

[3] A. Ayoub and F. C. Filippou. Mixed formulation of nonlinear steel-concrete composite beam element. *Journal of Structural Engineering*, 126(3):371–381, Mar. 2000.

[4] J.-M. Battini and C. Pacoste. Co-rotational beam elements with warping effects in instability problems. *Computer Methods in Applied Mechanics and Engineering*, 191(17-18):1755–1789, Feb. 2002.

[5] F. Boyer and D. Primault. Finite element of slender beams in finite transformations: a geometrically exact approach. *International Journal for Numerical Methods in Engineering*, 59(5):669–702, Dec. 2003.

[6] A. Cardona and M. Geradin. A beam finite element non-linear theory with finite rotations. *International Journal for Numerical Methods in Engineering*, 26(11):2403–2438, Nov. 1988.

[7] M. Chadha and M. D. Todd. The mathematical theory of a higher-order geometrically-exact beam with a deforming cross-section. *International Journal of Solids and Structures*, 202:854–880, Oct. 2020.

[8] G. R. Cowper. The shear coefficient in timoshenko's beam theory. *Journal of Applied Mechanics*, 33(2):335–340, June 1966.

[9] M. Crisfield. A consistent co-rotational formulation for non-linear, three-dimensional, beam-elements. *Computer Methods in Applied Mechanics and Engineering*, 81(2):131–150, Aug. 1990.

[10] M. A. Crisfield and G. Jelenić. Objectivity of strain measures in the geometrically exact three-dimensional beam theory and its finite-element implementation. *Proceedings of the Royal Society of London. Series A: Mathematical, Physical and Engineering Sciences*, 455(1983):1125–1147, Mar. 1999.

[11] L. Duan and J. Zhao. A geometrically exact cross-section deformable thin-walled beam finite element based on generalized beam theory. *Computers & Structures*, 218:32–59, July 2019.

[12] C. Felippa and B. Haugen. A unified formulation of small-strain corotational finite elements: I. theory. *Computer Methods in Applied Mechanics and Engineering*, 194(21-24):2285–2335, June 2005.

[13] S. Ghosh and D. Roy. Consistent quaternion interpolation for objective finite element approximation of geometrically exact beam. *Computer Methods in Applied Mechanics and Engineering*, 198(3-4):555–571, Dec. 2008.

[14] Y. Goto, Y. Watanabe, T. Kasugai, and M. Obata. Elastic buckling phenomenon applicable to deployable rings. *International Journal of Solids and Structures*, 29(7):893–909, 1992.

[15] G. Jelenić and M. Crisfield. Geometrically exact 3d beam theory: implementation of a strain-invariant finite element for statics and dynamics. *Computer Methods in Applied Mechanics and Engineering*, 171(1-2):141–171, Mar. 1999.

[16] R. Kouhia and M. Tuomala. Static and dynamic analysis of space frames using simple timoshenko type elements. *International Journal for Numerical Methods in Engineering*, 36(7):1189–1221, Apr. 1993.

[17] S. Krenk. *Non-linear modeling and analysis of solids and structures*. Cambridge University Press, Cambridge, UK New York, 2009. ISBN 978-0521830546.

[18] D. Magisano, L. Leonetti, and G. Garcea. Isogeometric analysis of 3d beams for arbitrarily large rotations: Locking-free and path-independent solution without displacement DOFs inside the patch. *Computer Methods in Applied Mechanics and Engineering*, 373:113437, Jan. 2021.

[19] J. Mäkinen. Total lagrangian reissner's geometrically exact beam element without singularities. *International Journal for Numerical Methods in Engineering*, 70(9):1009–1048, 2007.

[20] C. Meier, A. Popp, and W. A. Wall. An objective 3d large deformation finite element formulation for geometrically exact curved kirchhoff rods. *Computer Methods in Applied Mechanics and Engineering*, 278:445–478, Aug. 2014.

[21] C. Meier, A. Popp, and W. A. Wall. A locking-free finite element formulation and reduced models for geometrically exact kirchhoff rods. *Computer Methods in Applied Mechanics and Engineering*, 290:314–341, June 2015.

[22] C. Meier, A. Popp, and W. A. Wall. Geometrically exact finite element formulations for slender beams: Kirchhoff–love theory versus simo–reissner theory. *Archives of Computational Methods in Engineering*, 26(1):163–243, July 2017.

[23] B. Nour-Omid and C. Rankin. Finite rotation analysis and consistent linearization using projectors. *Computer Methods in Applied Mechanics and Engineering*, 93(3):353–384, Dec. 1991.

[24] F. C. Park and B. Ravani. Smooth invariant interpolation of rotations. *ACM Transactions on Graphics*, 16(3):277–295, July 1997.

[25] C. Rankin and B. Nour-Omid. The use of projectors to improve finite element performance. *Computers & Structures*, 30 (1-2):257–267, Jan. 1988.

[26] E. Reissner. On one-dimensional finite-strain beam theory: The plane problem. *Zeitschrift für angewandte Mathematik und Physik ZAMP*, 23(5):795–804, Sept. 1972.

[27] M. Ritto-Corrêa and D. Camotim. Work-conjugacy between rotation-dependent moments and finite rotations. *International Journal of Solids and Structures*, 40(11):2851–2873, 2003.

[28] I. Romero. The interpolation of rotations and its application to finite element models of geometrically exact rods. *Computational Mechanics*, 34(2), Apr. 2004.

[29] J. Rong, Z. Wu, C. Liu, and O. Brüls. Geometrically exact thin-walled beam including warping formulated on the special euclidean group SE(3). *Computer Methods in Applied Mechanics and Engineering*, 369:113062, Sept. 2020.

[30] C. Sansour and W. Wagner. Multiplicative updating of the rotation tensor in the finite element analysis of rods and shells - a path independent approach. *Computational Mechanics*, 31(1-2):153–162, May 2003.

[31] C. Sansour, T. L. Nguyen, and M. Hjiaj. An energy-momentum method for in-plane geometrically exact euler-bernoulli beam dynamics. *International Journal for Numerical Methods in Engineering*, 102(2):99–134, Jan. 2015.

[32] M. V. B. Santana. *Tailored Corotational Formulations for the Nonlinear Static and Dynamic Analysis of Bistable Structures*. PhD thesis, Université libre de Bruxelles, Brussels, Belgium, 2019.

[33] H. Santos, P. Pimenta, and J. Moitinho de Almeida. Hybrid and multi-field variational principles for geometrically exact three-dimensional beams. *International Journal of Non-Linear Mechanics*, 45(8):809–820, 2010.

[34] H. A. F. A. Santos and J. P. M. de Almeida. Equilibrium-based finite-element formulation for the geometrically exact analysis of planar framed structures. *Journal of Engineering Mechanics*, 136(12):1474–1490, Dec. 2010.

[35] H. A. F. A. Santos, P. M. Pimenta, and J. P. M. Almeida. A hybrid-mixed finite element formulation for the geometrically exact analysis of three-dimensional framed structures. *Computational Mechanics*, 48(5):591–613, June 2011.

[36] A. Saritas and F. C. Filippou. Inelastic axial-flexure–shear coupling in a mixed formulation beam finite element. *International Journal of Non-Linear Mechanics*, 44(8):913–922, Oct. 2009.

[37] S. W. Shepperd. Quaternion from rotation matrix. *Journal of Guidance and Control*, 1(3):223–224, May 1978.

[38] J. Simo. A finite strain beam formulation. the three-dimensional dynamic problem. part i. *Computer Methods in Applied Mechanics and Engineering*, 49(1):55–70, May 1985.

[39] J. Simo and L. Vu-Quoc. A three-dimensional finite-strain rod model. part II: Computational aspects. *Computer Methods in Applied Mechanics and Engineering*, 58(1):79–116, Oct. 1986.

[40] V. Sonneville, A. Cardona, and O. Brüls. Geometric interpretation of a non-linear beam finite element on the lie group SE(3). *Archive of Mechanical Engineering*, 61(2):305–329, Aug. 2014.

[41] V. Sonneville, A. Cardona, and O. Brüls. Geometrically exact beam finite element formulated on the special euclidean group. *Computer Methods in Applied Mechanics and Engineering*, 268:451–474, Jan. 2014.

[42] V. Sonneville, O. Brüls, and O. A. Bauchau. Interpolation schemes for geometrically exact beams: A motion approach. *International Journal for Numerical Methods in Engineering*, 112(9):1129–1153, 2017.

[43] A. Treven and M. Saje. Integrating rotation and angular velocity from curvature. *Advances in Engineering Software*, 85: 26–42, July 2015.

[44] O. Weeger, S.-K. Yeung, and M. L. Dunn. Fully isogeometric modeling and analysis of nonlinear 3d beams with spatially varying geometric and material parameters. *Computer Methods in Applied Mechanics and Engineering*, 342:95–115, Dec. 2018.

[45] O. Weeger, B. Narayanan, and M. L. Dunn. Isogeometric shape optimization of nonlinear, curved 3d beams and beam structures. *Computer Methods in Applied Mechanics and Engineering*, 345:26–51, Mar. 2019.

[46] G. Yoshiaki, W. Yasuhito, K. Toshihiro, and O. Makoto. Elastic buckling phenomenon applicable to deployable rings. *International Journal of Solids and Structures*, 29(7):893–909, 1992.

[47] D. Zupan and M. Saje. Finite-element formulation of geometrically exact three-dimensional beam theories based on interpolation of strain measures. *Computer Methods in Applied Mechanics and Engineering*, 192(49-50):5209–5248, Dec. 2003.

[48] E. Zupan and M. Saje. Integrating rotation from angular velocity. *Advances in Engineering Software*, 42(9):723–733, Sept. 2011.